NANO LETTERS
Cite This: Nano Lett. XXXX, XXX, XXX−XXX
Letter
pubs.acs.org/NanoLett

In Situ Investigation on the Nanoscale Capture and Evolution of Aerosols on Nanofibers

Rufan Zhang,[†] Bofei Liu,[†] Ankun Yang,[†] Yangying Zhu,[†] Chong Liu,[†] Guangmin Zhou,[†] Jie Sun,[†] Po-Chun Hsu,[†] Wenting Zhao,[†] Dingchang Lin,[†] Yayuan Liu,[†] Allen Pei,[†] Jin Xie,[†] Wei Chen,[†] Jinwei Xu,[†] Yang Jin,[†] Tong Wu,[†] Xuanyi Huang,[†] and Yi Cui*[,†,‡]

[†]Department of Materials Science and Engineering, Stanford University, Stanford, California 94305, United States

[‡]Stanford Institute for Materials and Energy Sciences, SLAC National Accelerator Laboratory, 2575 Sand Hill Road, Menlo Park, California 94025, United States

Supporting Information

ABSTRACT: Aerosol-induced haze problem has become a serious environmental concern. Filtration is widely applied to remove aerosols from gas streams. Despite classical filtration theories, the nanoscale capture and evolution of aerosols is not yet clearly understood. Here we report an in situ investigation on the nanoscale capture and evolution of aerosols on polyimide nanofibers. We discovered different capture and evolution behaviors among three types of aerosols: wetting liquid droplets, nonwetting liquid droplets, and solid particles. The wetting droplets had small contact angles and could move, coalesce, and form axisymmetric conformations on polyimide nanofibers. In contrast, the nonwetting droplets had a large contact angle on polyimide nanofibers and formed non-axisymmetric conformations. Different from the liquid droplets, the solid particles could not move along the nanofibers and formed dendritic structures. This study provides an important insight for obtaining a deep understanding of the nanoscale capture and evolution of aerosols and benefits future design and development of advanced filters.

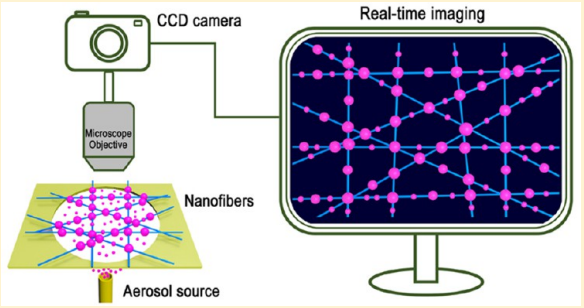

KEYWORDS: *PM2.5, filtration, nanofibers, aerosol, capture, in situ*

Clean air is an important aspect of sustainability. In recent years, particulate matter (PM) pollution has become a serious political, scientific, and public concern in many developing countries due to its significant impact on the living environments and public health.[1−8] Particularly, $PM_{2.5}$, defined as PM with aerodynamic diameter below 2.5 μm, can penetrate human bronchi, lungs, and even enter alveolar cells due to its small size, thus posing a serious threat to human health.[9−15] Among the various strategies proposed for $PM_{2.5}$ removal, the direct removal of $PM_{2.5}$ by high-efficiency air filters has been shown to be very effective.[8,16−23] Currently, filtration is also extensively applied in many other industrial and domestic fields, such as in nuclear power, semiconductor manufacturing, airplane cabin air-cleaning, pharmaceutical processing, and hospital environment.[24] According to the classical filtration theories, aerosol particles are captured by fibers through direct interception, Brownian diffusion, inertial impact, gravity settling, or electrostatic deposition (see Supporting Figure S1a),[25] depending on gas velocity, particle sizes, fiber diameters, and so forth.[24,26] It was also found that the surface chemistry and electrostatic potential of fibers play key roles in the high-efficiency capture of aerosols.[8] Despite the successful interpretation of filtration by the classical theories, the essential mechanism and the dynamic capture and evolution processes of aerosols, especially at the nanoscale, are not yet fully understood. Additionally, according to the Knudsen number used for describing flow regimes, the gas around nanofibers with diameter of 100−300 nm is in the transition flow regime (see Figure S1b−f and Table S1).[24,25] The classical filtration theories are inadequate for describing filtration in the transition flow regime due to the inapplicability of the Naiver−Stokes equation and the complexity of solving the Boltzmann equation.[24]

Aerosols can be categorized into solid and liquid aerosols, for which the filtration mechanisms are accordingly different. Previous works were mainly focused on filtration of solid aerosols, while studies on filtration of liquid aerosols were inadequate.[24] Furthermore, past studies on aerosol filtration were mainly based on ex situ and bulk analysis methods, which cannot well preserve the in situ and dynamic information on the capture and evolution of aerosols. Tiny aerosols tend to aggregate and only mean values are presented in the conventional methods.[27] Moreover, many proposed mathematical models of filtration are empirical or semiempirical, which

Received: November 3, 2017
Revised: December 14, 2017
Published: January 3, 2018

DOI: 10.1021/acs.nanolett.7b04673
Nano Lett. XXXX, XXX, XXX−XXX

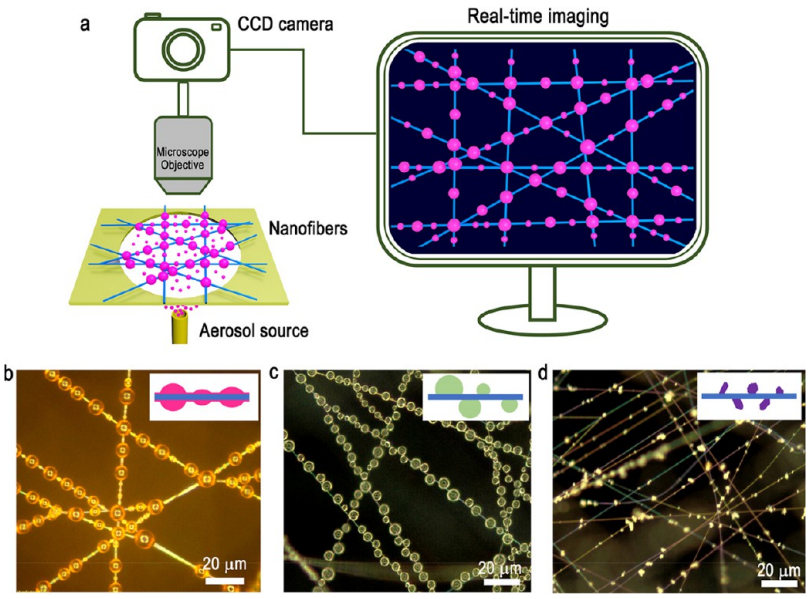

Figure 1. Schematic illustration of the in situ investigation on the nanoscale capture and evolution of aerosols on polyimide nanofibers and the typical images of different types of aerosols. (a) Illustration of the experimental setup. (b–d) Images of the in situ capture of (b) wetting droplets, (c) nonwetting droplets, and (d) solid particles by the nanofibers. Insets: Illustrations of the formation of wetting droplets, nonwetting droplets, and solid particles on the nanofibers, respectively.

cannot precisely describe the actual and complex capture behaviors and evolution processes of aerosols.[24−26,28] Here, we report an in situ investigation on the nanoscale capture and evolution process of different aerosols on polyimide nanofibers. Three types of aerosols were investigated: wetting liquid droplets, nonwetting liquid droplets, and solid particles. They showed distinct capture and evolution behaviors, arising from their different properties, for example, fluidity, viscosity, specific surface energy, and so forth. This in situ investigation provides new insights for understanding the filtration mechanisms of different aerosols at the nanoscale.

It was found in our previous study that electrospun polyimide nanofibers with diameter of 200−300 nm exhibited excellent $PM_{2.5}$ capture capability.[17] Besides, polyimide nanofibers also have high mechanical strength and can work at high temperature, exhibiting great advantages for fabricating high-efficiency air filter. Thus, we choose polyimide nanofibers as a platform to conduct the in situ investigation on the nanoscale capture and evolution of aerosols on nanofibers. The polyimide nanofibers were fabricated via electrospinning (Supporting Figure S2). Polyimide nanofibers with a low packing density were fabricated in this study to facilitate the observation of the capture process of individual aerosols. As shown in Figure 1a, a thin polyimide nanofiber network was placed under an optical microscope. A controllable aerosol source was placed under the nanofiber network. The capture of aerosols was controlled by tuning the gas flux from the source. The real-time capture of aerosols was recorded by a CCD camera connected to a computer. Three typical types of aerosols were investigated: wetting liquid droplets (Figure 1b), nonwetting liquid droplets (Figure 1c), and solid particles (Figure 1d). These aerosols showed distinct properties and capture behaviors. The wetting droplets had small contact angles on polyimide nanofibers and formed axisymmetric conformations on the nanofibers upon contact with them (inset of Figure 1b). The nonwetting liquid droplets had large contact angles on polyimide nanofibers and only formed nonaxisymmetric conformations (inset of Figure 1c). The conformation difference between wetting and nonwetting droplets resulted from the difference between their surface tension.[29] In contrast, the solid aerosols did not have regular shapes and instead formed dendritic structures on the nanofibers (inset of Figure 1d).

Smoke from biomass burning is one common aerosol source.[17] It has been shown in our previous study that most kinds of smoke from biomass burning contain a large amount of tiny oil-type droplets (concentration: $10^6 \sim 10^{10}/m^3$).[30] Here we took the oil droplets in cigarette smoke as an example to study the capture of wetting liquid droplets based on the following advantages: (i) cigarette smoke contains a large amount of tar droplets with diameters ranging from 0.1 to 3 μm, which are uniformly dispersed in smoke and serve as an ideal example of $PM_{2.5}$ aerosols; (ii) it is easy to control the flux of cigarette smoke for the precise investigation on the dynamic capture of tar droplets; and (iii) the tar droplets can wet polyimide nanofibers and gradually solidify within 0.5−1 h in ambient conditions and are thus favorable for further ex situ characterizations.

Figure 2a shows a schematic illustration of the capture, mobility, coalescence, and growth of wetting oil droplets from cigarette smoke on polyimide nanofibers. With the feeding of cigarette smoke, the oil droplets in the smoke were immediately captured upon contact with the nanofibers (Figure 2b), forming axisymmetric structures. It was reported that when a liquid droplet of definite volume was placed on a thin cylindrical fiber of definite radius, the conformation of the droplet was determined by the contact angle (gravity is not taken into consideration for length scales much smaller than the capillary length).[29] Generally, three distinct cases of conformation can occur when a droplet is placed on a cylindrical fiber (Supporting Figure S3):[31] (i) film flow (Figure S3a, but not very common, generally broken into distinct droplets due to the Plateau−Rayleigh instability[32] to reduce the surface area and the surface energy); (ii) a series of axisymmetric droplets (Figure S3b, usually connected by a film with a thickness on the

DOI: 10.1021/acs.nanolett.7b04673
Nano Lett. XXXX, XXX, XXX−XXX

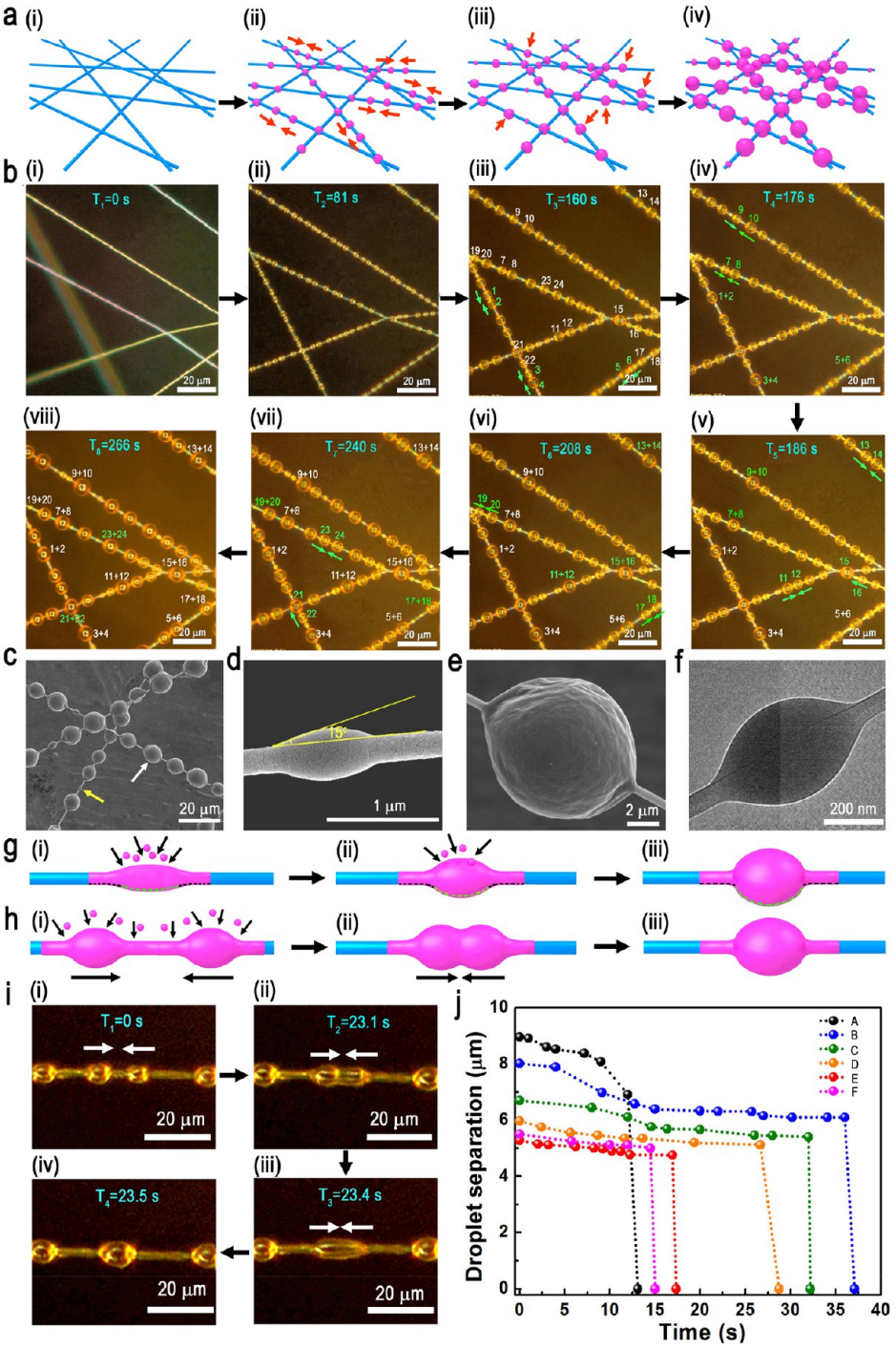

Figure 2. Capture, mobility, coalescence, and growth of oil droplets from cigarette smoke on polyimide nanofibers. (a) Schematic illustration of the capture, mobility, coalescence, and growth of oil droplets on polyimide nanofibers. a(i) A pristine polyimide nanofiber network. a(ii) The network begin to collect oil droplets with small diameters. a(iii) The adjacent captured droplets coalesce with each other. a(iv) The diameters of the droplets grow larger and larger. (b) Real-time imaging of the capture, mobility, coalescence, and growth of oil droplets on polyimide nanofibers. The numbers shown in these figures refer to the particles which will coalesce. (c–e) SEM and (f) TEM images of solid particles evolved by oil droplets from cigarette smoke after solidification. (g) Schematic illustration showing the process of new droplets merging into the pre-existing larger droplets on nanofibers. g(i) Small droplets begin to add onto a pre-existing droplet on the nanofiber. g(ii) and g(iii) The pre-existing droplet grow larger and larger with more small droplets being added in. The dashed black and green lines indicate the concave and convex sections of the outline of the longitudinal cross section of a droplet, respectively. (h) Schematic illustration of the coalescence process of adjacent oil droplets on nanofibers. h(i) Small droplets begin to add into two adjacent pre-existing droplets. h(ii) The two pre-existing droplets begin to connect with each other with more small droplets being added in. h(iii) The two-pre-existing droplets become a new larger one. i(i)–i(iv) The real-time images of the coalescence process of adjacent oil droplets on a nanofiber at different time. (j) The evolution of spatial separations of six pairs of droplets (labeled as A, B, C, D, E and F) on the nanofibers during the coalescence of adjacent droplets.

DOI: 10.1021/acs.nanolett.7b04673
Nano Lett. XXXX, XXX, XXX–XXX

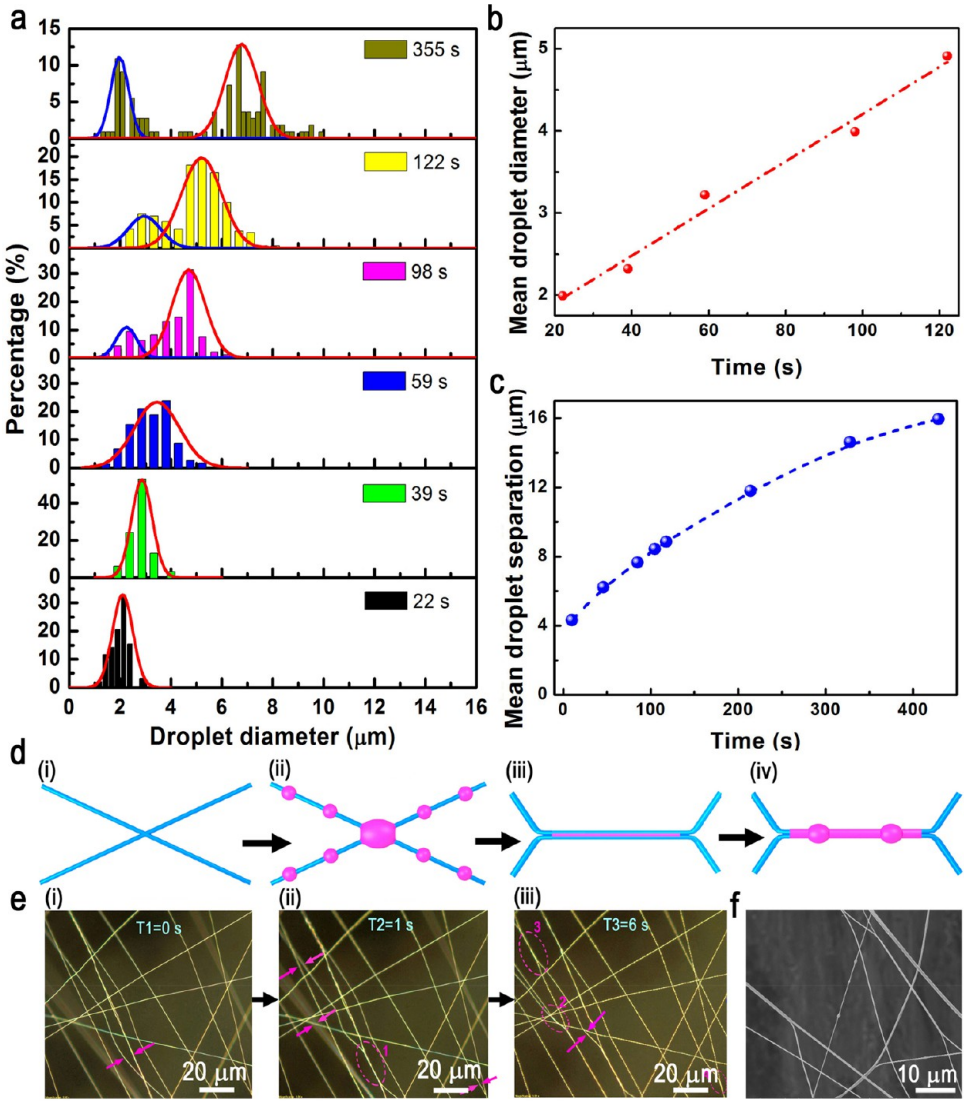

Figure 3. Diameter distribution of oil droplets from cigarette smoke on polyimide nanofibers and the adhesion of adjacent nanofibers. (a) The evolution of the diameter distribution of oil droplets. (b) The change of mean diameters of oil droplets over time. (c) The change of the mean droplet separations with time. (d) Schematic illustration of the adhesion of adjacent nanofibers caused by the capillary force of oil droplets between adjacent nanofibers. d(i) A pair of crossed nanofibers. d(ii) Some droplets are captured by the nanofibers. d(iii) The strong capillary force of oil droplets between two adjacent nanofibers causes the fibers to firmly adhere to each other. d(iv) With more droplets being captured by the two nanofibers, the coalesced nanofibers are completely coated by a layer of liquid and new droplets with larger diameters begin to appear on them. (e) Time-lapse images showing the adhesion of adjacent nanofibers by the oil droplets (indicated by four images labeled as i, ii, iii, and iv). The purple arrows and dashed ellipses indicate the nanofibers adhered together. (f) SEM image of adhered nanofibers.

order of nm); and (iii) nonaxisymmetric droplets (Figure S3c).[30,31] When the contact angle between the droplets and the fiber is small, the conformation of the droplets is symmetric with respect to the fiber axis. In contrast, when the contact angle is sufficiently large, a nonaxisymmetric conformation appears, which is more stable than the axisymmetric conformation. The specific surface energy of tar droplets (20−25 mJ/m^2 at 25−60 °C) is much lower than that of polyimide nanofibers (37−53 mJ/m^2 at room temperature), rendering a relatively higher adhesion between them and a relatively small contact angle of tar droplets on polyimide nanofibers (Figure 2c), thus favorable for the formation of axisymmetric conformation. The oil droplets captured on the nanofibers gradually became solid particles after 0.5−1 h in ambient conditions, which maintained stable at room temperature for several weeks (Figure S4). Figure 2c−f shows the SEM and TEM images of solid particles evolved from tar droplets in cigarette smoke, which well preserved the initial shapes of tar droplets before solidification. Additionally, droplets with different volumes presented different shapes on nanofibers (Figure 2c−e and S5) or at nanofiber-junctions (Figure S6). These shape variations were mainly due to the competition between the surface tension of droplets and the adhesion between droplets and nanofibers (see Supporting Text S1 and S2 for detailed discussion).

The volumes of oil droplets increased in two ways during the capture process. First, small droplets from the source were continuously added to the existing larger ones on the nanofibers (Figure 2g). Second, adjacent pairs of droplets often coalesced to form new ones with larger volumes (Figure 2h,i). As mentioned above (Figure S3b), there was a thin liquid film connecting the adjacent oil droplets. With more and more

DOI: 10.1021/acs.nanolett.7b04673
Nano Lett. XXXX, XXX, XXX−XXX

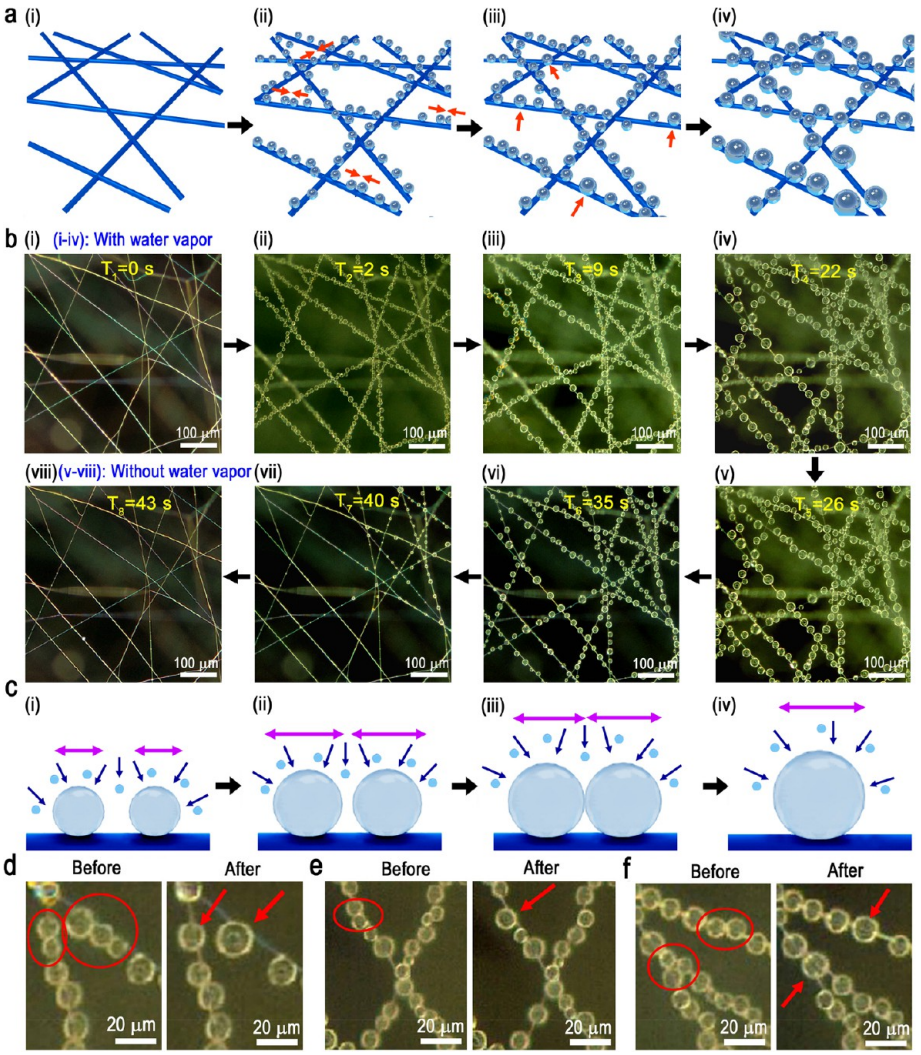

Figure 4. Capture of water droplets on polyimide nanofibers. (a) Schematic illustration of water droplet capture on polyimide nanofibers. a(i) A pristine polyimide nanofiber network. a(ii) The network begin capture water droplets with small diameters. a(iii) The captured small droplets begin to grow and coalesce with each other. a(iv) With more droplets being captured and coalesced with each other, the diameters of water droplets captured on this network become larger and larger. (b) Snapshots of real- time water droplet capture (i–iv) and evaporation (v–viii) process on polyimide nanofibers. From (i) to (iv), more and more small droplets are captured by the nanofibers and many of them coalesce with each other. From (v) to (viii), the diameters of water droplets become smaller and smaller and many of them disappear. (c) Schematic illustration of the coalescence of adjacent water droplets. c(i) Two adjacent water droplets. c(ii) With new small droplets being added, the two droplets begin to grow into larger ones. c(iii) With the increase of the diameter of the two droplets, their interspace becomes smaller and smaller. c(iv) Finally, the two droplets coalesce with each other. (d–f) Real-time images of the coalescence of adjacent water droplets.

small droplets merging into the existing ones and the thin films between them (Figure 2h,i), both the droplet diameter and the film thickness increased, breaking the equilibrium state between the liquid film and adjacent droplets. The surface tension of adjacent droplets overcame the adhesion between the droplets and nanofibers, thus driving adjacent droplets to coalesce and form new ones with larger volumes to reach a more stable state (Figure 2h(ii) and (iii)). The thin liquid film, which acted like a "bridge", played a key role in the coalescence of adjacent droplets. The coalescence of adjacent droplets is a universal phenomenon in the capture of wetting droplets by nanofibers. With the continuous capturing of new droplets, more pairs of adjacent droplets gradually coalesced with continuous increases in sizes. Additionally, six pairs of adjacent droplets were selected to investigate the evolution of their separations during the coalescence. As shown in Figure 2j, for most cases of droplet coalescence there were little or even no visible changes in the droplet separations for a relatively long time before the coalescence occurred. With the continuous addition of new droplets, the droplet separations suddenly decreased in a very short time (usually within 0.5 s), indicating the coalescence occurred.

We further investigated the diameter distribution of oil droplets from cigarette smoke. As shown in Figure 3a, the diameter distribution of the droplets captured by the nanofibers was a typical Gaussian distribution, which was very narrow at the initial capture stage (22 s) and had mean diameter of about 2.1 μm. With more droplets captured and coalesced, the diameter distribution broadened and the mean diameter increased. Moreover, with more small droplets captured by the nanofibers, two peaks appeared on the diameter distribution curve (98 s). Finally, the diameter distribution became very broad and the distance between the two peaks also increased (355 s). Figure 3b,c shows that both the mean droplet

DOI: 10.1021/acs.nanolett.7b04673
Nano Lett. XXXX, XXX, XXX–XXX

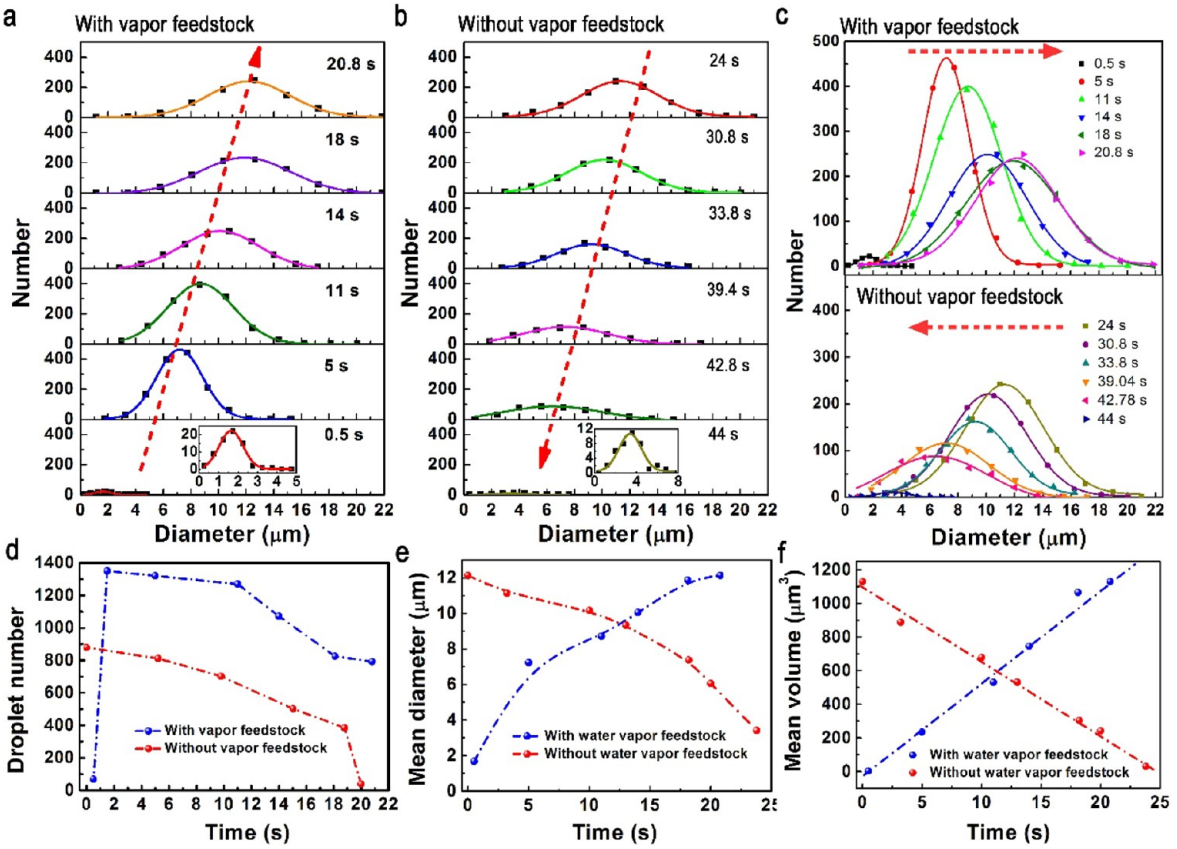

Figure 5. Diameter distribution of water droplets on polyimide nanofibers with and without water vapor feeding. (a) Number and diameter distribution variation during the capture of water droplets with water vapor feeding. (b) Number and diameter distribution variation during the evaporation of water droplets without water vapor feeding. (c) Comparison of number and diameter distribution of water droplets with and without water vapor feeding. (d–f) The variation of the droplet number (d), mean diameters (e), and mean volume (f) during the capture and evaporation of water droplets.

diameters and the droplet separations increased with the increase of the capture time. In addition to cigarette smoke, several other kinds of smoke from burning incense, wood, barbecue, and so forth, also contains a large amount of oil-type droplets, which show similar behaviors (Supporting Figure S7). Moreover, for the nanofiber networks with high packing densities and the nanofiber separations on the same order of magnitude with the droplet sizes, the captured droplets were in the form of small pools covering nanofibers or in the form of a combination of both droplets and pools/bridges between nanofibers after a long capture time (Supporting Figure S8).

The strong capillary force of oil droplets between two adjacent nanofibers also caused the fibers to firmly adhere to each other. The capillary force of liquids between nanofibers can be expressed as $F = 2\gamma l^*$, where γ is the surface tension and l^* is the contact line length.[33] As shown in Figure 3d, with the continuous capture of oil droplets the adjacent nanofibers quickly adhered to each other, during which the droplets filled in the gaps between the nanofibers. In general, long adjacent nanofibers with small intersection angles, large droplets sizes and numbers, and low tautness of nanofibers are favorable for the formation of adhered nanofibers with large adhesion lengths. The droplet-induced adhesion of adjacent nanofibers is a common phenomenon during the capture of wetting droplets (Figure 3e,f and Figure S9). The adhesion of adjacent nanofibers is not desired for the high-efficiency capture of aerosols. As shown in Figure S10, the adhesion of adjacent nanofibers "compressed" the initial three-dimensional nanofiber networks into a two-dimensional nanofiber mesh, which significantly reduced the pathway length of aerosols inside the filters and thus decreased the capture chances of aerosol particles. As shown in our previous work,[17] compared with thick nanofibers, thin nanofibers have higher available specific surface areas and provide higher aerosol capture efficiency.

To study the capture process of nonwetting droplets on polyimide nanofibers, we selected water as an example since the as-fabricated polyimide nanofibers exhibited typical hydrophobic properties (Figure S11 and Table S2). Water collection of spider silk has been reported previously.[34] Water has a specific surface energy (i.e., surface tension) of 72 mJ/m^2 at room temperature and 50 mJ/m^2 at 100 °C, which is much higher than that of many oil-type liquids and polyimide nanofibers. Figure 4a shows an illustration of how water droplets were captured by the polyimide nanofibers. In order to precisely control the numbers and sizes of water droplets, we used water vapor as the source. The water vapor flow was a mixture of water vapor and numerous tiny water droplets (0.1–1 μm). Once the water vapor reached the nanofibers, it immediately condensed on the nanofibers and formed water droplets. Additionally, the pre-existing water droplets in the gas flow also attached to the nanofibers. The water droplets had a large contact angle on polyimide nanofibers (Supporting Figure S12).Contrary to the axisymmetric structure of oil droplets on polyimide nanofibers, the water droplets had only a small portion of their surfaces attached to the polyimide nanofibers, and formed a nonaxisymmetric conformation. Figure 4b shows

DOI: 10.1021/acs.nanolett.7b04673
Nano Lett. XXXX, XXX, XXX–XXX

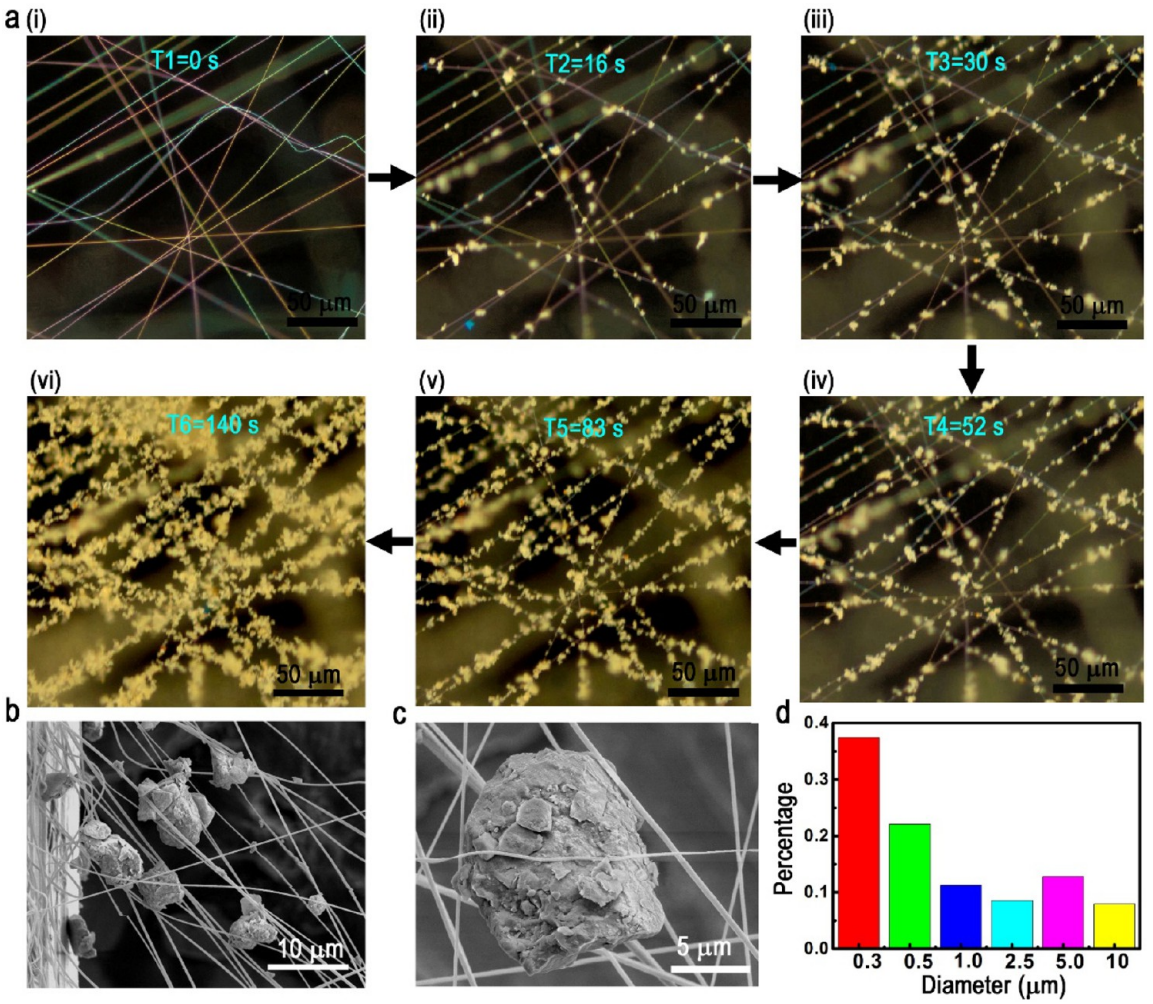

Figure 6. The capture, morphology, and size distribution of dust particles. (a) Snapshots of the real-time capture of dust particles on polyimide nanofibers. From (i) to (vi), more and more dust nanoparticles are captured by the nanofibers and they gradually form many dendrite-like structures. (b,c) SEM images of captured dust particles. (d) Size distribution of dust particles on nanofibers.

the real-time capture process of the water droplet on polyimide nanofibers. After feeding the water vapor for only 1−4 s, a large amount of tiny water droplets formed on the nanofibers (Figure 4b(i) and (ii)). The diameters of the droplets grew very quickly with the continuous feeding of water vapor due to condensation (Figure 5b(iii)). Meanwhile, the adjacent water droplets coalesced to form larger ones to minimize their surface energy (Figure 4a(ii), (iii), and 4d−f). The coalescence of water droplets manifested differently from that of oil droplets. First, adjacent but separated water droplets did not move toward each other, but instead grew large until they contacted and coalesced. This suggests there might not be a liquid film on the fiber between adjacent droplets (Figure S3c) because thin liquid films tend to be unstable when the liquid−vapor surface tension is high. With the continuous feeding of water vapor, the diameters of existing water droplets continuously increased, which reduced the distances between adjacent droplets (Figure 4c(i−iii). The adjacent droplets immediately coalesced once their surfaces came into contact (Figure 4c(iv)). Moreover, the coalescence were observed to synchronously occur among three or more water droplets at one time (Figure 4d,f), which was different from that of oil droplets.

The water droplets also exhibited another different characteristic from that of oil droplets investigated in this study. After we stopped feeding the water vapor, the high-temperature micron-sized water droplets could quickly evaporate into the ambient environment owing to their extremely large specific surface areas and high saturation vapor pressure (i.e., high Laplace pressure), especially at such small radius. As shown in Figure 4b(v) and (vi), the diameter of the water droplets decreased sharply after only 5 s without water vapor feeding. This fast evaporation benefits the regeneration of filters after capturing water or other similar liquid aerosols. Furthermore, the number of water droplets also decreased rapidly (Figure 4b(vii)). Most of the water droplets quickly evaporated into the air and finally almost nothing was left on the nanofibers (Figure 4b(viii)). In addition, the water droplets also caused the adhesion of adjacent nanofibers but only within a much smaller region and with a different morphology from that caused by oil droplets. As shown in Figure S13, the adhered nanofibers were only weakly attached to each other by van der Waals interactions after the complete evaporation of water. There are two reasons for this difference. First, for contact angle <90 (wetting liquids), the pressure of the liquid bridge between two fibers is negative, that is, it pulls fibers together. In contrast, for contact angles >90, the pressure of the liquid bridge is positive, that is, it repels the fibers from each other. Thus, the adhesion of nanofibers caused by water droplets was much less than that caused by oil

DOI: 10.1021/acs.nanolett.7b04673
Nano Lett. XXXX, XXX, XXX−XXX

droplets. Second, the oil droplets from smoke could solidify in ambient conditions, firmly fixing the adhered nanofibers together.

We further studied the distribution of the droplet diameters during the condensation and evaporation processes. The diameter distribution of water droplets was also a typical Gaussian distribution. As shown in Figure 5a, at the initial stage (0.5 s) of the water droplet capture, only very few droplets with small diameters (1−3 μm) appeared on the nanofibers. After only 3−5 s, there was a sharp increase in the number of droplets. The mean diameter of droplets at 5 s was around 7.5 μm. From 5 to 20.8 s, the mean diameter continued to increase, however the droplet number decreased due to droplet coalescence (Figure 5a,c−e). The mean droplet volume also showed a continuous increase with vapor feeding (Figure 5f). Subsequently, when the water vapor feeding was turned off, the droplet number, the mean diameter and the mean volume decreased sharply owing to the rapid evaporation of water droplets (Figure 5b-f).

Finally, we studied the capture process of solid aerosols on polyimide nanofibers. We utilized soil dust particles as an example because of their abundance in nature. The dust particles were milled into nanosized particles and then carried by gas flow to pass through the polyimide nanofibers. Once the dust particles got into contact with the nanofibers, they immediately attached to and accumulated on the nanofibers. The dust particles were mainly captured by the nanofibers via van der Waals interaction (Figure 6a(i) and (ii)). With continuous feeding of the dust flow, more and more solid particles were captured. The newly captured particles attached to both the uncovered pairs of the nanofibers and the existing attached particles. Finally, numerous dendrite-like structures formed with the continuous capture of dust particles (Figure 6a(iii)−(vi)). Unlike the liquid droplets, the solid particles could not move along the nanofibers and thus could not coalesce with each other. The morphology of the dust particles was stochastic and without a regular shape (Figure 6b,c), which was different from that of liquid droplets. In addition, their size distribution was much broader and highly random (Figure 6d). Compared with oil droplets, the adhesion of the dust particles with the nanofibers was weak and some of the captured particles could even be blown away by the drag forces of a strong gas flow. We also investigated the capture of other solid particles, such as CuO nanowires (Figure S14a), TiO_2 nanoparticles (Figure S14b), carbon nanotube agglomerates (Figure S14c), and graphene nanosheets (Figure S14d), and found that they exhibited similar capture behaviors. The difference between the liquid and solid aerosols is related to the fundamental difference between liquids and solids, that is, the ability to flow. The liquid droplets can move and coalesce along the nanofibers. Both the wetting and nonwetting droplets showed the quasi-spherical shapes and their size distribution was narrow. In contrast, the solid particles did not have regular shapes and their size distribution was very broad. They created permanent intrusive dendritic structures.

In conclusion, we conducted the in situ investigation on the nanoscale capture and evolution of three types of aerosols on polyimide nanofibers, including wetting droplets, nonwetting droplets, and solid particles. The filtration of these aerosols exhibited distinct behaviors. For the liquid droplets, the capture and evolution was related to the surface tension. The wetting droplets had a small contact angle on polyimide nanofibers and formed axisymmetric conformations. The wettability facilitated the capture of wetting droplets on the nanofibers. Besides, they could also adhere the adjacent nanofibers to each other. In comparison, the nonwetting droplets had a large contact angle on the polyimide nanofibers and formed nonaxisymmetric conformations on them. The solid particles could neither completely wrap the nanofibers, nor move along them, but only attached to them with a small part of their surface by weak van der Waals forces, forming dendritic structures on the nanofibers. This study provides new insight for the understanding of the nanoscale filtration mechanisms of different kinds of aerosols and guide future design of high efficiency advanced filters. For example, different types of aerosols require different structure design and surface modification of fibers to tune the specific surface energy so as to enhance the wettability and adhesion of target aerosols on the nanofibers.

Methods. *1. Fabrication of Polyimide Nanofibers by Electrospinning.* The polyimide nanofibers were fabricated through electrospinning of polyimide *N*,*N*-dimethylformamide (DMF) solution. The solution system for the polymers used in this study was 15 wt % polyimide resin (CAS #62929-02-6, Alfa Aesar) in DMF (EMD Millipore). A 1 mL syringe with a 22-gauge needle tip was used to load the polymer solution and connected to a voltage supply (ES30P-5W, Gamma High Voltage Research). A syringe pump (KD Scientific) was used to pump the solution out of the needle tip. The nanofibers were collected by a grounded copper mesh. The wire diameter of the copper mesh was 0.011 in., and the mesh size was 18 × 16. During electrospinning, the nanofibers would lie across the mesh hole to form the air filter.

2. In Situ Observation System Setup. A copper mesh-supported thin polyimide nanofiber network with size of about 5 cm × 5 cm was placed under a high-resolution optical microscope. A controllable customized aerosol source was placed under the nanofiber network. The capture of aerosols was controlled by tuning the gas flux from the source. The real-time capture of aerosols was recorded by a CCD camera connected to a computer. Three typical types of aerosols were investigated: wetting liquid droplets, nonwetting liquid droplets, and solid particles. The wetting liquid droplets were produced from the smoke by burning a cigarette. The nonwetting liquid droplets were produced by heating the water to boiling point. The solid particles were produced by blowing the milled soil dust with an air gas flow.

3. Other Characterizations. The SEM images were taken by FEI XL30 Sirion SEM with an acceleration voltage of 5 kV for imaging. The TEM images and EELS data were collected with an FEI Titan TEM with the acceleration voltage of 300 kV.

■ ASSOCIATED CONTENT

Supporting Information

The Supporting Information is available free of charge on the ACS Publications website at DOI: 10.1021/acs.nanolett.7b04673.

Supporting Texts S1−S3; Supporting Figures S1−S15; Supporting Tables S1 and S2 (PDF)

■ AUTHOR INFORMATION

Corresponding Author

*E-mail: yicui@stanford.edu.

ORCID

Rufan Zhang: 0000-0003-1774-0550

Ankun Yang: 0000-0002-0274-4025

DOI: 10.1021/acs.nanolett.7b04673
Nano Lett. XXXX, XXX, XXX−XXX

Dingchang Lin: 0000-0002-9354-5952
Allen Pei: 0000-0001-8930-2125
Jin Xie: 0000-0002-6270-1465
Wei Chen: 0000-0001-7701-1363
Yi Cui: 0000-0002-6103-6352

Author Contributions

R.Z., B.L., A.Y., and Y.Z. contributed equally to this work. Y.C. and R.Z. conceived the concept of the project. R.Z. designed and performed the main experiments and wrote the manuscript. B.L., A.Y., and Y.Z. participated in the conception, data analysis, figure design and preparation of the manuscript. All authors analyzed the data and contributed to the discussion.

Notes

The authors declare no competing financial interest.

■ ACKNOWLEDGMENTS

Part of this work was performed at the Stanford Nano Shared Facilities (SNSF) and Stanford Nanofabrication Facility (SNF).

■ REFERENCES

(1) Huang, R.; Zhang, Y.; Bozzetti, C.; Ho, K.; Cao, J.; Han, Y.; Daellenbach, K. R.; Slowik, J. G.; Platt, S. M.; Canonaco, F.; et al. *Nature* **2014**, *514*, 218−222.
(2) Nel, A. *Science* **2005**, *308*, 804−806.
(3) Mahowald, N. *Science* **2011**, *334*, 794−796.
(4) Horton, D. E.; Skinner, C. B.; Singh, D.; Diffenbaugh, N. S. *Nat. Clim. Change* **2014**, *4*, 698−703.
(5) Watson, J. G. *J. Air Waste Manage. Assoc.* **2002**, *52*, 628−713.
(6) Streets, D. G.; Wu, Y.; Chin, M. *Geophys. Res. Lett.* **2006**, *33*, 1−4.
(7) Andreae, M.; Rosenfeld, D. *Earth-Sci. Rev.* **2008**, *89*, 13−41.
(8) Liu, C.; Hsu, P.-C.; Lee, H.-W.; Ye, M.; Zheng, G.; Liu, N.; Li, W.; Cui, Y. *Nat. Commun.* **2015**, *6*, 6205.
(9) Betha, R.; Behera, S. N.; Balasubramanian, R. *Environ. Sci. Technol.* **2014**, *48*, 4327−4335.
(10) Wu, S.; Deng, F.; Wei, H.; Huang, J.; Wang, X.; Hao, Y.; Zheng, C.; Qin, Y.; Lv, H.; Shima, M.; et al. *Environ. Sci. Technol.* **2014**, *48*, 3438−3448.
(11) Brook, R. D.; Rajagopalan, S.; Pope, C. A.; Brook, J. R.; Bhatnagar, A.; Diez-Roux, A. V.; Holguin, F.; Hong, Y.; Luepker, R. V.; Mittleman, M. A.; et al. *Circulation* **2010**, *121*, 2331−2378.
(12) Anenberg, S. C.; Horowitz, L. W.; Tong, D. Q.; West, J. *Environ. Health Persp.* **2010**, *118*, 1189−1195.
(13) Timonen, K. L.; Vanninen, E.; De Hartog, J.; Ibald-Mulli, A.; Brunekreef, B.; Gold, D. R.; Heinrich, J.; Hoek, G.; Lanki, T.; Peters, A.; et al. *J. Exposure Sci. Environ. Epidemiol.* **2006**, *16*, 332−341.
(14) Zhao, S.; Chen, L.; Li, Y.; Xing, Z.; Du, K. *Atmosphere* **2015**, *6*, 234−254.
(15) Hoek, G.; Krishnan, R. M.; Beelen, R.; Peters, A.; Ostro, B.; Brunekreef, B.; Kaufman, J. D. *Environ. Health* **2013**, *12*, 1−15.
(16) Li, P.; Zong, Y.; Zhang, Y.; Yang, M.; Zhang, R.; Li, S.; Wei, F. *Nanoscale* **2013**, *5*, 3367−3372.
(17) Zhang, R.; Liu, C.; Hsu, P.-C.; Zhang, C.; Liu, N.; Zhang, J.; Lee, H. R.; Lu, Y.; Qiu, Y.; Chu, S.; et al. *Nano Lett.* **2016**, *16*, 3642−3649.
(18) Yang, A.; Cai, L.; Zhang, R.; Wang, J.; Hsu, P.-C.; Wang, H.; Zhou, G.; Xu, J.; Cui, Y. *Nano Lett.* **2017**, *17*, 3506−3510.
(19) Xu, J.; Liu, C.; Hsu, P.-C.; Liu, K.; Zhang, R.; Liu, Y.; Cui, Y. *Nano Lett.* **2016**, *16*, 1270−1275.
(20) Zhang, Y.; Yuan, S.; Feng, X.; Li, H.; Zhou, J.; Wang, B. *J. Am. Chem. Soc.* **2016**, *138*, 5785−5788.
(21) Gong, G.; Zhou, C.; Wu, J.; Jin, X.; Jiang, L. *ACS Nano* **2015**, *9*, 3721−3727.
(22) Wang, S.; Zhao, X.; Yin, X.; Yu, J.; Ding, B. *ACS Appl. Mater. Interfaces* **2016**, *8*, 23985−23994.
(23) Chen, Y.; Zhang, S.; Cao, S.; Li, S.; Chen, F.; Yuan, S.; Xu, C.; Zhou, J.; Feng, X.; Ma, X.; et al. *Adv. Mater.* **2017**, *29*, 1606221.
(24) Li, P.; Wang, C.; Zhang, Y.; Wei, F. *Small* **2014**, *10*, 4543−4561.
(25) Chen, C.-Y. *Chem. Rev.* **1955**, *55*, 595−623.
(26) Yang, C. *Chin. J. Chem. Eng.* **2012**, *20*, 1−9.
(27) Feng, X.; Dang, Z.; Huang, W.; Shao, L.; Li, W. *J. Atmos. Chem.* **2009**, *64*, 37−51.
(28) Xu, B.; Wu, Y.; Cui, P. *Particuology* **2014**, *13*, 60−65.
(29) Carroll, B. *Langmuir* **1986**, *2*, 248−250.
(30) Zhang, R.; Liu, C.; Zhou, G.; Sun, J.; Liu, N.; Hsu, P.-C.; Wang, H.; Qiu, Y.; Zhao, J.; Wu, T.; et al. *Nano Res.* **2017**, 1−11.
(31) Mullins, B. J.; Agranovski, I. E.; Braddock, R. D.; Ho, C. M. *J. Colloid Interface Sci.* **2004**, *269*, 449−458.
(32) Haefner, S.; Benzaquen, M.; Bäumchen, O.; Salez, T.; Peters, R.; McGraw, J. D.; Jacobs, K.; Raphaël, E.; Dalnoki-Veress, K. *Nat. Commun.* **2015**, *6*, 7409.
(33) Duprat, C.; Protiere, S.; Beebe, A.; Stone, H. *Nature* **2012**, *482*, 510−513.
(34) Zheng, Y.; Bai, H.; Huang, Z.; Tian, X.; Nie, F.-Q.; Zhao, Y.; Zhai, J.; Jiang, L. *Nature* **2010**, *463*, 640−643.

DOI: 10.1021/acs.nanolett.7b04673
Nano Lett. XXXX, XXX, XXX−XXX